Nondiffracting Bessel plasmons

Carlos J. Zapata-Rodríguez,[1,*] **Slobodan Vuković,**[2] **Milivoj R. Belić,**[3] **David Pastor,**[1] **and Juan J. Miret**[4]

[1]*Department of Optics, University of Valencia, Dr. Moliner 50, 46100 Burjassot, Spain*
[2]*Institute of Physics, University of Belgrade, Pegrevica 118, 11080 Zemun, Serbia*
[3]*Texas A & M University at Qatar, P.O. Box 23874, Doha, Qatar*
[4]*Department of Optics, Pharmacology and Anatomy, University of Alicante, P.O. Box 99, Alicante, Spain*

[*]*carlos.zapata@uv.es*

Abstract: We report on the existence of nondiffracting Bessel surface plasmon polaritons (SPPs), advancing at either superluminal or subluminal phase velocities. These wave fields feature deep subwavelength FWHM, but are supported by high-order homogeneous SPPs of a metal/dielectric (MD) superlattice. The beam axis can be relocated to any MD interface, by interfering multiple converging SPPs with controlled phase matching. Dissipative effects in metals lead to a diffraction-free regime that is limited by the energy attenuation length. However, the ultra-localization of the diffracted wave field might still be maintained by more than one order of magnitude.

OCIS codes: (240.6680) Surface plasmons; (350.5500) Propagation.

References and links

1. J. Durnin, "Exact solutions for nondiffracting beams. I. The scalar theory," J. Opt. Soc. Am. A **4**, 651–654 (1987).
2. J. Durnin, J. J. Miceli, and J. H. Eberly, "Diffraction-free beams," Phys. Rev. Lett. **58**, 1499–1501 (1987).
3. V. Garces-Chavez, D. McGloin, H. Melville, W. Sibbett, and K. Dholakia, "Simultaneous micromanipulation in multiple planes using a self-reconstructing light beam," Nature **419**(6903), 145–147 (2002).
4. J. Jezek, T. Cizmar, V. Nedela, and P. Zemanek, "Formation of long and thin polymer fiber using nondiffracting beam," Opt. Express **14**(19), 8506–8515 (2006).
5. M. K. Bhuyan, F. Courvoisier, P. A. Lacourt, M. Jacquot, L. Furfaro, M. J. Withford, and J. M. Dudley, "High aspect ratio taper-free microchannel fabrication using femtosecond Bessel beams," Opt. Express **18**(2), 566–574 (2010).
6. B. Hafizi, E. Esarey, and P. Sprangle, "Laser-driven acceleration with Bessel beams," Phys. Rev. E **55**(3, Part B), 3539–3545 (1997).
7. Y. Kartashov, V. Vysloukh, and L. Torner, "Rotary solitons in Bessel optical lattices," Phys. Rev. Lett. **93**(9), 093904 (2004).
8. M. A. Porras, G. Valiulis, and P. D. Trapani, "Unified description of Bessel X waves with cone dispersion and tilted pulses," Phys. Rev. E **68**, 016613 (2003).
9. C. J. Zapata-Rodríguez and M. A. Porras, "X-wave bullets with negative group velocity in vacuum," Opt. Lett. **31**(23), 3532–3534 (2006).
10. T. Wulle and S. Herminghaus, "Nonlinear optics of Bessel beams," Phys. Rev. Lett. **70**, 1401–1404 (1993).
11. L. Van Dao, K. B. Dinh, and P. Hannaford, "Generation of extreme ultraviolet radiation with a Bessel–Gaussian beam," Appl. Phys. Lett. **95**(13) (2009).
12. J. Fan, E. Parra, and H. Milchberg, "Resonant self-trapping and absorption of intense Bessel beams," Phys. Rev. Lett. **84**(14), 3085–3088 (2000).
13. P. Polesana, A. Couairon, D. Faccio, A. Parola, M. A. Porras, A. Dubietis, A. Piskarskas, and P. Di Trapani, "Observation of conical waves in focusing, dispersive, and dissipative Kerr media," Phys. Rev. Lett. **99**(22), 223902 (2007).
14. D. Faccio and P. Di Trapani, "Conical-wave nonlinear optics: From Raman conversion to extreme UV generation," Laser Phys. **18**(3), 253–262 (2008).

#151987 - $15.00 USD Received 28 Jul 2011; revised 2 Sep 2011; accepted 2 Sep 2011; published 22 Sep 2011

15. H. Kano, D. Nomura, and H. Shibuya, "Excitation of surface-plasmon polaritons by use of a zeroth-order Bessel beam," Appl. Opt. **43**(12), 2409–2411 (2004).
16. K. J. Moh, X. C. Yuan, J. Bu, S. W. Zhu, and B. Z. Gao, "Radial polarization induced surface plasmon virtual probe for two-photon fluorescence microscopy," Opt. Lett. **34**(7), 971–973 (2009).
17. Q. Zhan, "Evanescent Bessel beam generation via surface plasmon resonance excitation by a radially polarized beam," Opt. Lett. **31**(11), 1726–1728 (2006).
18. A. Bouhelier, F. Ignatovich, A. Bruyant, C. Huang, G. C. d. Francs, J.-C. Weeber, A. Dereux, G. P. Wiederrecht, and L. Novotny, "Surface plasmon interference excited by tightly focused laser beams," Opt. Lett. **32**(17), 2535–2537 (2007).
19. W. Chen and Q. Zhan, "Realization of an evanescent Bessel beam via surface plasmon interference excited by a radially polarized beam," Opt. Lett. **34**(6), 722–724 (2009).
20. A. Shaarawi, B. Tawfik, and I. Besieris, "Superluminal advanced transmission of X waves undergoing frustrated total internal reflection: the evanescent fields and the Goos–Hanchen effect," Phys. Rev. E **66**(4, Part 2), 046626 (2002).
21. S. Longhi, K. Janner, and P. Laporta, "Propagating pulsed Bessel beams in periodic media," J. Opt. B **6**, 477–481 (2004).
22. W. Williams and J. Pendry, "Generating Bessel beams by use of localized modes," J. Opt. Soc. Am. A **22**(5), 992–997 (2005).
23. C. J. Zapata-Rodríguez, M. T. Caballero, and J. J. Miret, "Angular spectrum of diffracted wave fields with apochromatic correction," Opt. Lett. **33**, 1753–1755 (2008).
24. A. V. Novitsky and L. M. Barkovsky, "Total internal reflection of vector Bessel beams: Imbert-Fedorov shift and intensity transformation," J. Opt. A **10**(7), 075006 (2008).
25. V. N. Belyi, N. S. Kazak, S. N. Kurilkina, and N. A. Khilo, "Generation of TE- and TH-polarized Bessel beams using one-dimensional photonic crystal," Opt. Commun. **282**(10), 1998–2008 (2009).
26. D. Mugnai and P. Spalla, "Electromagnetic propagation of Bessel-like localized waves in the presence of absorbing media," Opt. Commun. **282**, 4668–4671 (2009).
27. G. Rui, Y. Lu, P. Wang, H. Ming, and Q. Zhan, "Evanescent Bessel beam generation through filtering highly focused cylindrical vector beams with a defect mode one-dimensional photonic crystal," Opt. Commun. **283**(10), 2272–2276 (2010).
28. C. J. Zapata-Rodríguez and J. J. Miret, "Diffraction-free beams in thin films," J. Opt. Soc. Am. A **27**, 663–670 (2010).
29. C. Zapata-Rodríguez and J. Miret, "Subwavelength nondiffractting beams in multilayered media," Appl. Phys. A **103**, 699–702 (2011).
30. S. Longhi and D. Janner, "X-shaped waves in photonic crystals," Phys. Rev. B **70**, 235123 (2004).
31. O. Manela, M. Segev, and D. N. Christodoulides, "Nondiffracting beams in periodic media," Opt. Lett. **30**, 2611–2613 (2005).
32. J. J. Miret and C. J. Zapata-Rodríguez, "Diffraction-free beams with elliptic Bessel envelope in periodic media," J. Opt. Soc. Am. B **25**, 1–6 (2008).
33. J. J. Miret and C. J. Zapata-Rodríguez, "Diffraction-free propagation of subwavelength light beams in layered media," J. Opt. Soc. Am. B **27**(7), 1435–1445 (2010).
34. J. J. Miret, D. Pastor, and C. J. Zapata-Rodriguez, "Subwavelength surface waves with zero diffraction," J. Nanophoton. **5**, 051801 (2011).
35. A. Salandrino and D. N. Christodoulides, "Airy plasmon: a nondiffracting surface wave," Opt. Lett. **35**, 2082–2084 (2010).
36. P. Yeh, *Optical Waves in Layered Media* (Wiley, 1988).
37. S. M. Vukovic, Z. Jaksic, and J. Matovic, "Plasmon modes on laminated nanomembrane-based waveguides," J. Nanophoton. **4**, 041770 (2010).
38. H. M. Antia, *Numerical methods for scientists and engineers* (Tata McGraw-Hill Publishing Company Limited, 1991).
39. J. Elser, V. A. Podolskiy, I. Salakhutdinov, and I. Avrutsky, "Nonlocal effects in effective-medium response of nanolayered metamaterials," Appl. Phys. Lett. **90**(19), 191109 (2007).
40. J. D. Joannopoulos, S. G. Johnson, J. N. Winn, and R. D. Meade, *Photonic crystals. Molding the flow of light* (Princeton University Press, 2008).

1. Introduction

In 1987 Durnin presented experimental evidence on the generation of a high-intensity focused wave field that kept its transverse spot size unaltered for much longer than its Rayleigh range [1, 2]. Such a localized radiation mode was called the nondiffracting beam (also the diffraction-free beam), due to its apparent violation of the natural beam spreading induced by

#151987 - $15.00 USD Received 28 Jul 2011; revised 2 Sep 2011; accepted 2 Sep 2011; published 22 Sep 2011

free-space propagation. It propagated in a linear medium and was not to be confused with the spatial solitons, which commonly appear in nonlinear media. In due course of time this sort of waves became mostly known as the Bessel Beams (BBs), since the profile of the transverse field followed, in the vast majority of practical realizations, a Bessel function of the first kind. Since in the domain of spatial frequencies the wave vectors of the constitutive plane waves were wrapped around a conical surface, similar to the Cerenkov radiation, this lead to a new appellative of conical waves, employed a few times by some authors. Additionally, for pulsed beams, the spatiotemporal evolution represented in a meridional plane that contains the BB axis is shaped as a cross; in this case one preferably speaks of the X-waves.

All these names reflect unique features of this sort of wave fields. In fact, the self-healing property, which has not been mentioned yet, plays a relevant role in numerous applications, such as the optical manipulation of micro-sized particles [3], the fabrication of long polymer fibers induced by the photopolymerization [4] and microchanneling by structural modification in glass materials [5], the enhancement of energy gain in inverse free electron lasers and inverse Cerenkov accelerators [6], and the generation of Bessel photonic lattices imprinted in photorefractive crystals [7]. The possibility of independently tuning the phase and group velocities (GVs) of a BB opens the possibility of a number of applications in nonlinear optics [8, 9]. In particular, a number of phenomena was observed: frequency-doubling [10] and high-order harmonics in the extreme ultraviolet [11] using BBs, resonant self-trapping of BBs in plasmas [12], the spontaneous formation of unbalanced BBs during ultrashort laser pulse filamentation in Kerr media [13], and high Raman conversion efficiency in the formation of GV-matched X-wave pulses [14].

The recent and fast development of plasmonics has propelled the irruption of BBs on the stage, with the excitation of surface plasmon polaritons (SPPs) in several applications. Kano *et al.* reported the first experimental result concerning an efficient excitation of local SPPs, by using the zeroth-order BB [15]. More recently, radially-polarized BBs have been demonstrated to provide the TM polarization required for the effective coupling to the SPPs, which can be used as a virtual probe for the two-photon fluorescence microscopy [16]. We point out that the evanescent BBs can be obtained irrespective of the transverse profile of the radially-polarized impinging beam [17–19]. In the initial case the incidence of the BB is placed normally to the MD interface, leading to the invariance of the transverse Bessel pattern. This property has been observed also in all-dielectric stratified structures [20–27]. In plasmon-driven evanescent BBs, however, the wave field experiences an on-axis variation, which follows an exponential decay. With this regard in mind, we remark that the intensity of a diffraction-free wave field that propagates in 1D structured media is rigorously flat if the beam injection into the photonic device is performed under grazing incidence [28, 29]. Nevertheless, the inherent anisotropy of the strati-formed media prevents the nondiffracting beam from exhibiting an azimuthally-symmetric amplitude distribution [30–34].

In this paper we demonstrate the existence of a SPP that evolves without distortion within an energy-attenuation length and whose in-plane profile traces a Bessel function along the transverse direction relative to the beam axis. This should be set apart from the evanescent BBs mentioned before, whose centro-symmetric amplitude distribution features converging and diverging waves on the metal/dielectric interface. Consequently, this type of subwavelength plasmonic field is free of diffraction on the flat surface and remains highly confined around the beam axis. With this result, it is proved that the recently introduced Airy plasmon is not the only nondiffracting surface plasmonic wave [35]. Fundamental differences between the surface waves and 2D waves are exemplified, to understand how unconfined sinusoidal waves, which are the counterpart of the conical waves in 2D, assist in the formation of highly-localized nondiffracting surface waves.

#151987 - $15.00 USD Received 28 Jul 2011; revised 2 Sep 2011; accepted 2 Sep 2011; published 22 Sep 2011

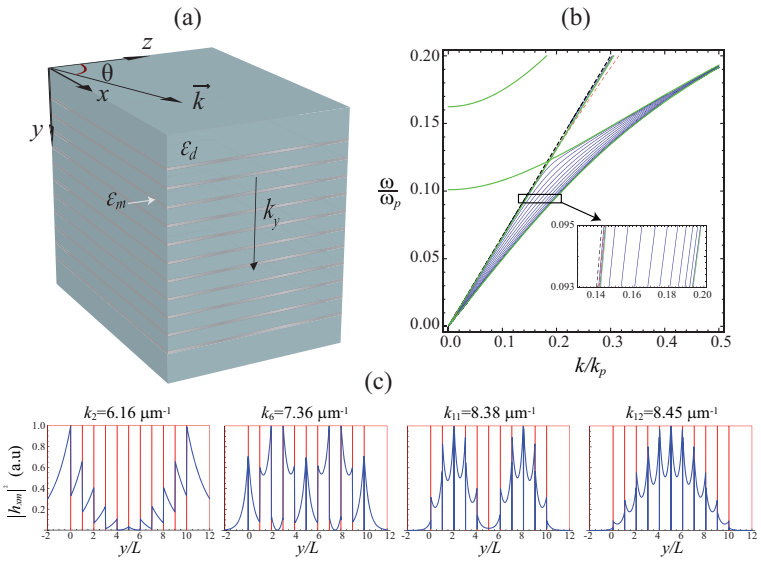

Fig. 1. (a) Geometry of the multilayered nanostructure; thin silver nanomembranes of $w_m =$ 10 nm are impressed into fused silica $\varepsilon_d = 2.25$ at a rate of 3.33 μm^{-1}. (b) Dispersion curves of guided modes for $N = 11$. Dashed red line is the dispersion of ordinary SPP; green lines represent bandgap edges. (c) Intensity distribution $|h_{xm}|^2$ for several modal solutions at $\lambda_0 = 1.55$ μm.

2. High-order plasmonic modes

We consider a monochromatic surface wave propagating with a wavevector k in a MD multilayered structure consisting of a finite number N of metallic layers and $N-1$ slabs of a dielectric material. The layers are alternatively placed and stacked around a solid cladding, as shown in Fig. 1(a). The widths of the metallic slabs and the dielectric slabs are denoted by w_m and w_d. The y axis is set perpendicular to the MD interfaces, and x and z axes are situated in one of the interface planes. A discrete function $\varepsilon(y)$ characterizes the relative dielectric constant of the stratified medium. Particularly, it takes a real value ε_d in the dielectric films and a complex-valued ε_m in the metallic layers. Material properties of metals can be appropriately described by the Drude-Lorentz model, from which the frequency-dependent permittivity follows the formula

$$\varepsilon_m(\omega) = 1 - \frac{\omega_p^2}{\omega(\omega + i\gamma)} \ . \tag{1}$$

Here ω_p is the plasma frequency of the metal and γ is the damping factor related to the losses in the material. For silver, $\omega_p = 12.9$ fs^{-1} and $\gamma = 0.08$ fs^{-1}. Without loss of generality we assume that ε_d also denotes the dielectric constant of the cladding.

A MD stratified medium commonly provides a number of electromagnetic field modes, which we identify by an index $m = \{1, 2, \cdots, M\}$. For convenience, we cast the magnetic field of each plasmonic mode as

$$\vec{H}_m(x,y,z) \quad = \quad \vec{h}_m(y) \exp\left[ik_m (z\cos\theta_m + x\sin\theta_m)\right] \tag{2}$$

where k_m is the wavenumber of the mth-order surface mode and θ_m determines its direction of propagation in the plane. The wavenumber k_m is frequently given in terms of the plasmonic

#151987 - $15.00 USD Received 28 Jul 2011; revised 2 Sep 2011; accepted 2 Sep 2011; published 22 Sep 2011

spatial frequency $k_p = c/\omega_p$. Furthermore, in order to excite surface resonances in the interfaces of our device, *p*-polarized waves should be employed. Therefore, we consider TM waves whose magnetic field is confined in the *xz* plane, that is $\vec{h}_m = (h_{xm}, 0, h_{zm})$. We point out that the magnetic field is solenoidal, leading to the equation $h_{zm} = -\tan\theta_m h_{xm}$. We conclude that the problem may be fully described in terms of the scalar wavefield h_{xm}, from which other electromagnetic components may be derived.

Using the standard matrix formulation for isotropic layered media, we can describe unambiguously the amplitude $h_{xm}(y)$ distributed inside our device. The general procedure may be followed from Ref. [33]. For a large number N of metallic strata, the periodic medium operates just as a photonic lattice whose unit cell translation matrix is here denoted by T. The 2×2 matrix T depends upon the wavenumber k_m of the surface plasmon, but it is otherwise independent of the angular coordinate θ_m. For an ideally unbounded photonic crystal, the values of k_m are determined by the dispersion equation [36]:

$$2\cos(k_{ym}L) = T_{11} + T_{22} \ , \tag{3}$$

where $L = w_d + w_m$ is the period of the lattice and k_{ym} is a Bloch wavenumber. As a consequence, the values of k_m are restricted to allowed bands, which emerge when the trace of T spans the region from -2 to 2, as depicted in Fig. 1(b). In the case presented we neglected material losses, by taking $\gamma = 0$; thus T became unimodular. Since the periodic structure is finite, solutions are derived from the equation $\left[T^N\right]_{11} = 0$, which is equivalent to [37]

$$(T_{11} - T_{22})\tan(Nk_{ym}L) + 2\sin(k_{ym}L) = 0 \ . \tag{4}$$

In the example considered $N = 11$. Now, the wavenumbers k_m form a discrete set of M real numbers. This is shown in Fig. 1(b) where we obtained $M = 12$ high-order SPPs. The modal field decays exponentially in the limit $|y| \to \infty$ and it may vary substantially within the stratified medium, as shown in Fig. 1(c). However, these surface waves are homogeneous in the *xz* plane, as shown in Eq. (2). In general, the larger the number N of layers, the higher the number $M = \max(m)$ of plasmonic modes sustainable in such a MD nanostructure.

3. Diffraction-free sinusoidal beams

Strictly speaking, the homogeneous surface wave disclosed in (2) represents a nondiffracting beam whose propagation constant k_m is governed by the MD multilayer. However, we may modify ad lib the spatial frequency $\beta \geq 0$ along the beam axis of a nondiffracting SPP, here taken to be the *z* axis, provided $\beta \leq k_m$. For that purpose we consider the superposition of two homogeneous surface plasmons of the same wavenumber k_m, but different directions of propagation, given by the angles $+\theta_m$ and $-\theta_m$, respectively, as shown in Fig. 2(a). The projections of the wave vectors onto the *z* axis coincide with $\beta = k_m \cos\theta_m$ leading to a phase front advancing at a velocity $v_p = \omega/\beta$ along such a direction. Assuming additionally that both plasmonic modes become equal in strength $|h_{xm}|$, the net flux of power along the *x* axis is zero. The resultant field $H_{xm} = h_{xm}(y)\exp(i\beta z)\cos(k_{xm}x + \varphi_m)$ yields Young fringes whose maxima are controlled by the spatial frequency $k_{xm} = k_m \sin\theta_m$ and the dephasing φ_m of the surface plasmons [see Fig. 2(b)].

We point out that the sinusoidal SPP has an effective mode index

$$n_{\text{eff}} \equiv \frac{c}{v_p} = \frac{\beta}{k_0}, \tag{5}$$

which is bounded by that of the surface wave, $n_m = k_m/k_0$, where $k_0 = 2\pi/\lambda_0$. In other words, the sinusoidal SPP runs faster than a single-mode SPP. In general, $0 < n_{\text{eff}} < \sqrt{\varepsilon_d}$, leading to a

#151987 - $15.00 USD Received 28 Jul 2011; revised 2 Sep 2011; accepted 2 Sep 2011; published 22 Sep 2011

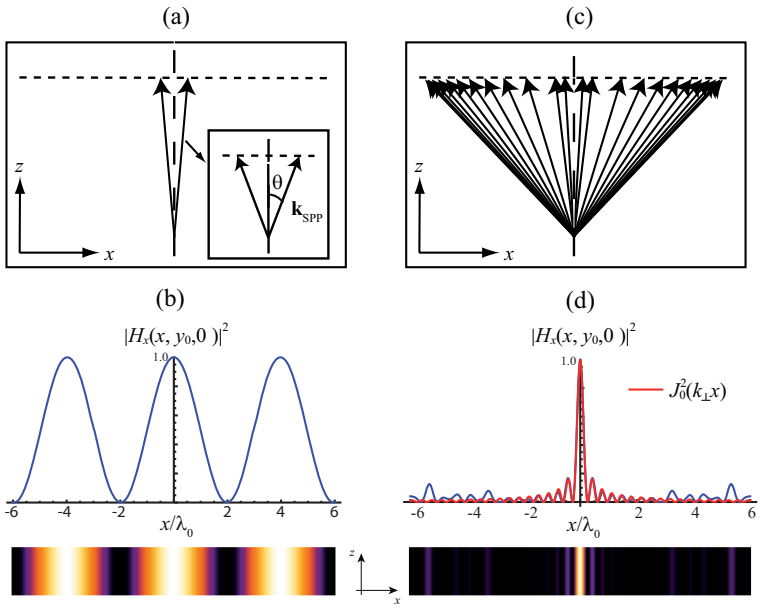

Fig. 2. Formation of a nondiffracting cos beam mediated by SPPs on a silver-fused silica interface: (a) Sketch of the wavevectors distribution and (b) contours of intensity $|H_x|^2$ in the xz plane at $\lambda_0 = 1.55\ \mu$m. Excitation of multiple high-order SPPs is schematically represented in (c) using here every high-order SPP involved. (d) Intensity distribution in the xz plane running with $M = 12$ modes. The quadrature (6) on the surface $y = y_0$ is performed for a Bessel function of $k_\perp = 5.90\ \mu\text{m}^{-1}$ shown in red. The propagation constant is $\beta = 6.12\ \mu\text{m}^{-1}$ in (b) and (d).

superluminal signal, if it is compared with a plane wave traveling through the bulk fused silica. It may happen, however, that $\sqrt{\varepsilon_d} < n_{\text{eff}} < n_m$, inducing a subluminal velocity of the phase fronts. This abnormal result is caused by the presence of the metallic aggregate and it cannot be found in diffraction-free beams propagating in bulk dielectric media. In our numerical simulations we have made use of a propagation constant $\beta = 6.12\ \mu\text{m}^{-1}$ which, in practical terms, is associated with a luminal effective-mode index $n_{\text{eff}} = 1.51 \gtrapprox \sqrt{\varepsilon_d}$ at telecoms wavelengths.

4. Ultra-confined modes

The nondiffracting sinusoidal beam driven by monomode SPPs is clearly unconfined [35]. Note that such a wave interference is practicable for any order m of the mode. Therefore, we may conceive a coherent superposition of plasmonic cosine waves exhibiting the same propagation constant β along the z axis, provided that $\beta \leq k_m$ for all m involved. This condition fixes the values of θ_m, as outlined in Fig. 2(c) for the twelve distinct SPPs. Moreover, localization around the beam axis, set on a given MD interface $y = y_0$ at $x = 0$, is achieved by adapting the individual dephases such that $\varphi_m = 0$, giving

$$H_x \quad = \quad \exp(i\beta z) \sum_{m=1}^{M} h_{xm}(y) \cos(k_{xm} x)\ . \tag{6}$$

The superposition proposed in Eq. (6) is not enough by itself to generate a localized wave field inside the MD device. For that purpose we manipulate the amplitudes $h_{xm}(y_0)$ in order to

#151987 - $15.00 USD Received 28 Jul 2011; revised 2 Sep 2011; accepted 2 Sep 2011; published 22 Sep 2011

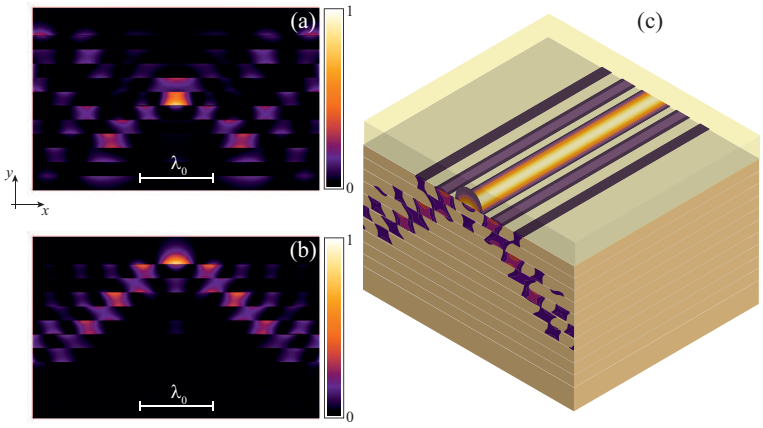

Fig. 3. (a) Intensity pattern of the nondiffracting Bessel plasmon in the *xy* plane for a phase matching at the top surface of the central layer. (b) The same as in (a) for a phase matching at the uppermost MD interface. (a) 3D view of the multilayered device and the surface BB generated in (b).

match their phases at the beam axis. Furthermore, we seek for values of $h_{xm}(y_0)$ leading to a field $H_x(x,y_0,0)$ to trace a Bessel profile. We may express the zeroth-order Bessel function as

$$J_0(k_\perp x) = \int_0^{k_\perp} f(k_\perp, k_x)\cos(k_x x)\,dk_x\ , \tag{7}$$

where $f = 2/\pi\sqrt{k_\perp^2 - k_x^2}$. For convenience we assume that the arbitrary frequency $k_\perp$ is higher than any k_{xm} involved. Our procedure is based on the fact that the integral (7) approaches the series expansion (6) given at $(x,y_0,0)$ by means of a numerical quadrature with preassigned nodes k_{xm} [38]. The solutions $h_{xm}(y_0) = f(k_\perp,k_{xm})\int L_m(k_x)\,dk_x$ of the quadrature, expressed in terms of the Lagrange polynomials L_m, provide a wave field through Eq. (6) whose intensity on the MD interface is approximately $J_0^2(k_\perp x)$. The resulting field is here called the nondiffracting Bessel plasmon. This is depicted in Fig. 2(d) using all $M = 12$ modes involved at $\lambda_0 = 1.55\ \mu$m. The central part of the waveform is accurately represented by the Bessel function, whose highest main peak has an intensity FWHM $\Delta_x = 0.38\ \mu$m. The error visible in the wings comes from difference between the finite series expansion and the integral involving Bessel function.

The validity of this procedure is evident near the beam axis for values of β close to $k_1 = \min(k_m)$, causing the coefficients $h_{xm}(y_0) \geq 0$ to be in phase. If the number M of modes becomes large, we may conveniently break up the integral (7) into several parts, leading to the well-known compound rules [38]. Occasionally, we may disregard some modal solutions in Eq. (6), without significant loss of accuracy. Finally, the error term of the quadrature formula decreases for $k_\perp$ approaching the maximum value of all k_{xm} involved, that is k_{xM}.

After following the procedure given above, the oscillatory superposition (6) yields the highest intensity achievable at $x = 0$ on the MD surface $y = y_0$. Under ordinary conditions it will not be found at a point out of the beam axis, where such a phase matching holds. As a consequence, a strong confinement of the plasmonic BB is expected to occur around $(x,y) = (0,y_0)$. Note, however, that nonlocality of high-order SPPs [39] leads to a considerable disparity in intensity from one interface to the other, as exhibited in Fig. 1(c). For instance, a gain in outlying interfaces is achieved in detriment to the central surfaces, by considering the SPP of propagation

#151987 - $15.00 USD Received 28 Jul 2011; revised 2 Sep 2011; accepted 2 Sep 2011; published 22 Sep 2011

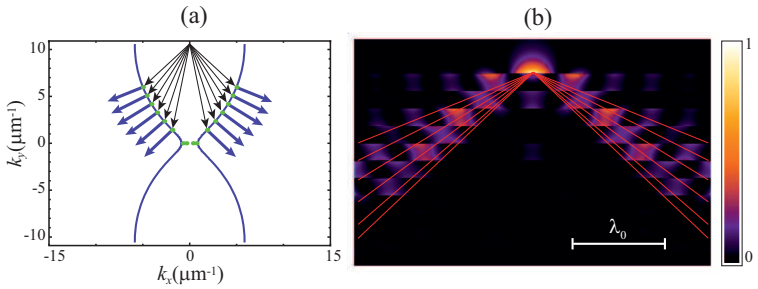

Fig. 4. (a) Dispersion contour for $\lambda_0 = 1.55\ \mu$m and resultant directions of $\vec{u}$ for the excited SPP modes. Thick arrows indicate group-velocity directions, and thin arrows stand for phase-velocity vectors whose origin is shifted to $k_y = \pi/L$ for clarity. (b) The same as Fig. 3(b), including directions of energy flow intersecting at the beam axis.

constant $k_2 = 6.16\ \mu\text{m}^{-1}$. We conclude that it is propitious for a phase matching at the cladding boundaries, but it leads to spurious sidelobes in the case when the beam axis is set around the center of the layered waveguide. Contrarily, the SPP of $k_{12} = 8.45\ \mu\text{m}^{-1}$ enhances the field in the central part of the metal-dielectric structure, which benefits the bright spots traveling on a MD interface near the midpoint. We point out that some SPPs will be useful for both cases, as displayed for $k_6 = 7.36\ \mu\text{m}^{-1}$, but others like $k_{11} = 8.38\ \mu\text{m}^{-1}$ might disable light confinement in the mentioned regions.

In Fig. 3 we represent $|H_x|^2$ derived from Eq. (6) when the phase matching is boosted at different surfaces of the metal-dielectric nanostructure. In Fig. 3(a) the phase matching is accomplished on the interface that belongs to the central silver film. For convenience we discarded 5 plasmonic modes with indices $m = \{1,2,7,9,11\}$, which induced a field localization out of the beam axis. The numerical quadrature was set for the BB that has a transverse frequency $k_\perp = 5.90\ \mu\text{m}^{-1}$. The anisotropic spot displays a subwavelength FWHM $\Delta y = 160$ nm along the y axis, and an in-plane FWHM $\Delta x = 416$ nm. In Fig. 3(b) the beam axis is relocated on the boundary of the MD device and the cladding. In this case we employed 8 different surface modes (from $m = 1$ to $m = 8$) for the Bessel quadrature, with $k_\perp = 5.20\ \mu\text{m}^{-1}$. As a consequence, the FWHM $\Delta x = 430$ nm results in a slightly higher value than that obtained above, otherwise $\Delta y = 113$ nm. This is also illustrated in Fig. 3(c) by means of the full 3D arrangement. Note that the transverse wave field in (a) is essentially different from (b), in spite of using roughly the same in-plane Bessel distribution.

The control of the field is initially established in the xz plane, however, out-of-plane intensity is determined by the geometry and materials composing the multilayered waveguide. The Bessel-like distribution along the x axis cannot be maintained in other directions, due to the intrinsic anisotropy of the stratified medium. Moreover, the field of the Bessel plasmon is enhanced along distinctive paths in the transverse xy plane. These characteristic directions are usually associated with those of the energy flow [40]. To obtain the lengthwise paths where the field is confined near the beam axis, we calculate the Poynting vector for each homogeneous SPP. This procedure is rendered possible by the following important result: The group velocity $\vec{u}_m = d\omega/d\vec{k}_{tm}$ represents the average Poynting vector in the xy plane divided by the average energy density for every Bloch mode of the MD lattice, where $\vec{k}_{tm} = (k_{xm}, k_{ym})$. Accordingly, the energy flux of the nondiffracting Bessel plasmon travels normally to the beam axis along the gradients provided from the dispersion contour.

Figure 4(a) shows the dispersion contour for the lossless device given in Fig. 1(a) at a fre-

#151987 - $15.00 USD Received 28 Jul 2011; revised 2 Sep 2011; accepted 2 Sep 2011; published 22 Sep 2011

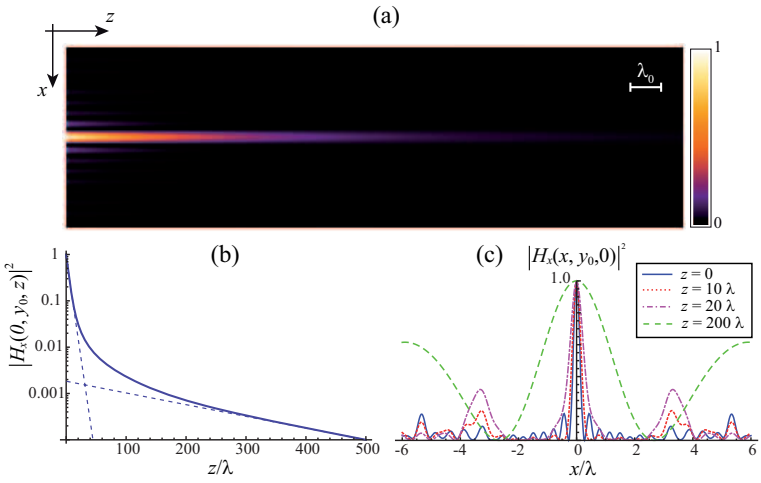

Fig. 5. Numerical experiment with $\gamma = 0.08$ fs^{-1} for silver. (a) Surface distribution of the initiated BB in the *xz* plane. (b) Evolution of the intensity along beam axis. The dashed line represents the asymptotic behavior of the on-axis intensity that is valid when a single long-range SPP contributes effectively in Eq. (6). (c) Transverse intensity distribution normalized at the beam axis for different propagation distances.

quency $\omega = 0.0942\omega_p$, that corresponds to the vacuum wavelength $\lambda_0 = 1.55\ \mu$m. The photonic band structure of this 1D MD crystal can be calculated numerically using Eq. (3). For each plasmonic Bloch mode we present a straight line whose slope s_m is governed by the gradient computed from the dispersion contour, that is the direction of the vector $\vec{u}_m$, as $s_m = [\vec{u}_m]_y / [\vec{u}_m]_x$. Note that the 1st- and 2nd-order SPPs are located in the bandgap of the periodic MD medium and therefore are excluded from the present analysis. The strongly scattering MD lattice modifies the dispersion relation of light so much that the dispersion contour is far from being circular. As a result, the velocities $\vec{u}_m$ involved are clumped into two classes, including low numerical aperture wavevectors whose slopes $\pm s_m$ do not differ substantially. In Fig. 4(b) we represent the straight lines intersecting on the beam axis where the phase matching is accomplished, as shown in Fig. 3(b). We verify that light is bounded primarily at regions marked by the streamlines of the Poynting vectors associated with each plasmonic mode.

5. Dissipation effects

Purely diffraction-free Bessel plasmons described above exist assuming an ideal conductor with $\gamma = 0$. Excitations of free electrons of real metals however suffer damping. Therefore, we consider now the case when γ in Eq. (1) is no longer zero and with it the SPP propagation constant k_m becomes complex. The traveling SPPs are damped with an energy attenuation length $l_m = [2\mathrm{Im}\,(k_m)]^{-1}$. As a consequence, the nondiffracting nature of plasmonic BBs is preserved, but each *m*th-order SPP contributing in the summation of Eq. (6) runs a distance shorter than its propagation length l_m. This effect is illustrated in Fig. 5(a). The phase fronts of the field H_x advance with a constant velocity, provided $\beta = \mathrm{Re}\,(k_m)\cos\theta_m$ is conserved. The modal angle θ_m brings to effect that each causal plasmonic signal travels its own distance l_m, to reach the beam axis at the *z* axis coordinate $l_m/\cos\theta_m$. In our numerical simulation $l_1 = 267\ \mu$m, $l_2 = 45.0\ \mu$m, and l_m decreases fast at higher *m*, up to $l_{11} = 3.09\ \mu$m and $l_{12} = 3.06\ \mu$m; however $\theta_m \ll 1$ leading to an incessant drop of higher *m*th-order terms taking part in the summation in Eq. (6).

#151987 - $15.00 USD Received 28 Jul 2011; revised 2 Sep 2011; accepted 2 Sep 2011; published 22 Sep 2011

Consequently, the on-axis intensity is reduced by a factor $1/e$ at $z = 6.8$ μm, as shown in Fig. 5(b), which is primarily determined by the energy attenuation lengths of the highest-order SPPs. Fig. 5(c) elucidates how the Bessel profile of the nondiffracting plasmon evolves toward a cosine amplitude distribution. This evidences that the 1st-order sinusoidal SPP contributes exclusively to the wave superposition (6) at sufficiently long distances.

6. Conclusions

In conclusion, we have demonstrated the existence of nondiffracting Bessel plasmons which, in difference to the Airy plasmons, travel along a straight trajectory. In our numerical simulations, light confinement is sustained in bulk fused silica, by inserting a silver thin-film aggregate with a period of $L = 0.30$ μm. We have analyzed a device including 11 nanomembranes of 10 nm each, operating at telecom wavelength $\lambda_0 = 1.55$ μm. A Bessel wave field with intensity FWHM $\Delta_x = 0.38$ μm is guided along the metal/dielectric flat interface at a propagation constant $\beta = 6.12$ μm^{-1}, leading to a luminal phase velocity $v_p = 0.66c$. The origin of this interesting phenomenon lies in the phase-matched excitation of superlattice of high-order SPPs. Dissipative effects in silver leads to a diffraction-free regime that is limited by energy attenuation length of $l = 6.8$ μm. However, localization about the beam axis is maintained along a range which is higher than l by more than one order of magnitude.

Acknowledgments

This research was funded by the Spanish Ministry of Science and Innovation under the project TEC2009-11635, and by the Qatar National Research Fund under the project NPRP 09-462-1-074. S.V. and M.R.B. wish to acknowledge the support for this work provided by Serbian Ministry of Education and Science through grant No. III 45016.

#151987 - $15.00 USD Received 28 Jul 2011; revised 2 Sep 2011; accepted 2 Sep 2011; published 22 Sep 2011